Clim Dyn (2012) 39:1001–1020
DOI 10.1007/s00382-011-1189-8

An ensemble estimation of the variability of upper-ocean heat content over the tropical Atlantic Ocean with multi-ocean reanalysis products

Jieshun Zhu · Bohua Huang · Magdalena A. Balmaseda

Received: 2 May 2011 / Accepted: 3 September 2011 / Published online: 17 September 2011

Abstract Current ocean reanalysis systems contain considerable uncertainty in estimating the subsurface oceanic state, especially in the tropical Atlantic Ocean. Given this level of uncertainty, it is important to develop useful strategies to identify realistic low-frequency signals optimally from these analyses. In this paper, we present an "ensemble" method to estimate the variability of upper-ocean heat content (HC) in the tropical Atlantic based on multiple-ocean reanalysis products. Six state-of-the-art global ocean reanalaysis products, all of which are widely used in the climate research community, are examined in terms of their HC variability from 1979 to 2007. The conventional empirical orthogonal function (EOF) analysis of the HC anomalies from each individual analysis indicates that their leading modes show significant qualitative differences among analyses, especially for the first modes, although some common characteristics are discernable. Then, the simple arithmetic average (or ensemble mean) is applied to produce an ensemble dataset, i.e., the EM analysis. The leading EOF modes of the EM analysis show quantitatively consistent spatial–temporal patterns with those derived from an alternative EOF technique that maximizes signal-to-noise ratio of the six analyses, which suggests that the ensemble mean generates HC fields with the noise reduced to an acceptable level. The quality of the EM analysis is further validated against AVISO altimetry sea level anomaly (SLA) data and PIRATA mooring station data. A regression analysis with the AVISO SLA data proved that the leading modes in the EM analysis are realistic. It also demonstrated that some reanalysis products might contain higher level of intrinsic noise than others. A quantitative correlation analysis indicates that the HC fields are more realistic in the EM analysis than in individual products, especially over the equatorial regions, with signals contributed from all ensemble members. A direct comparison with the HC anomalies derived from in situ temperature measurements showed that the EM analysis generally gets realistic HC variability at the five chosen PIRATA mooring stations. Overall, these results demonstrate that the EM analysis is a promising alternative for studying physical processes and possibly for initializing climate predictions.

Keywords Tropical Atlantic variability · Upper-ocean heat content · Multi-ocean reanalysis products · Ensemble estimation

J. Zhu (✉) · B. Huang
Center for Ocean–Land–Atmosphere Studies, Institute of Global Environment and Society, Calverton, MD, USA
e-mail: jieshun@cola.iges.org

B. Huang
Department of Atmospheric, Oceanic, and Earth Sciences, College of Science, George Mason University, Fairfax, VA, USA

M. A. Balmaseda
European Center for Medium-Range Weather Forecasts, Reading, UK

1 Introduction

Although sea surface temperature (SST) anomalies (SSTA) in the tropical Atlantic are generally weaker than those associated with El Niño/Southern Oscillation (ENSO) in the Pacific, their low-frequency fluctuations show large-scale patterns that are significantly linked with the climate fluctuations in the surrounding regions. For example, early studies have demonstrated that the precipitation over northeast Brazil (Hastenrath and Heller 1977; Moura and

Shukla 1981) and sub-Saharan Africa (Lamb 1978; Folland et al. 1986) are statistically associated with the so-called Atlantic meridional gradient mode, characterized by the fluctuation of the SST meridional gradient near the equator from interannual to decadal time scales, largely driven by off-equatorial SSTAs (e.g., Servain 1991; Nobre and Shukla 1996; Enfield and Mayer 1997). There is also evidence suggesting that the rainfall fluctuations on the Gulf of Guinea coast (Wagner and da Silver 1994) and in Angola (Hirst and Hastenrath 1983) are connected with the Atlantic equatorial mode, also referred to as the Atlantic Niño, characterized by anomalous warm and cold SSTAs in the Gulf of Guinea and the southeastern boundary (e.g., Servain et al. 1982; Carton and Huang 1994; Florenchie et al. 2004). Skillful prediction of these anomalous SST patterns at long-leads is the main challenge of climate forecasting in the Atlantic sector (Kushnir et al. 2006).

Previous studies have indicated that the oceanic subsurface memories play an important role in tropical Atlantic variability (TAV). The equatorial mode has been recognized as resulting from air-sea interaction, in which the displacement of the equatorial thermocline and propagation of the oceanic waves play a vital role (e.g., Handoh and Bigg 2000), much like its counterpart ENSO in the Pacific (Zebiak 1993; Carton and Huang 1994; Huang and Shukla 1997; Xie and Carton 2004). For the Atlantic meridional gradient mode, previous studies have indicated that accompanying the SST meridional variability generated by thermodynamic air-sea feedback (Chang et al. 1997; Xie 1999), there are important subsurface heat content changes forced by anomalous wind curl (Huang and Shukla 1997; Ruiz-Barradas et al. 2000; Joyce et al. 2004; Lee and Wang 2008). Huang et al. (1995) and Huang and Shukla (1997) argued that the propagation of the heat content anomalies into the equatorial waveguide may stimulate the equatorial mode and generate SSTAs in the southeastern Atlantic later on. Servain et al. (1999) also suggested that the meridional mode is linked to the equatorial mode almost simultaneously at both decadal and short-interannual (1–2 years) time scales, due to the latitudinal displacements of the inter-tropical convergence zone (ITCZ). On the other hand, Joyce et al. (2004) showed that the wind-driven meridional heat transport damps the meridional mode and affects the North Equatorial Countercurrent (NECC). Lee and Wang (2008) also argued that the SST-dipole induced wind stress curl generates a cross-equatorial gyre, which affects the meridional heat transport as well as the zonal SST gradient along the equator. Moreover, oceanic pathways, via the meridional overturning cells, have been suggested to give rise to the lower frequency components of the dipole SST pattern in the tropical Atlantic as a response to the changes in the high-latitude North Atlantic (Yang 1999; Dong and Sutton 2002; Xie and Carton 2004; Wen et al. 2009), in addition to the faster southward expansion of the extratropical anomalies by the wind-evaporation-SST (WES) feedback (Chiang and Bitz 2005; Mahajan et al. 2011). The WES feedback originating from the subtropical South Atlantic (e.g., Huang and Shukla 2005) also contributes to TAV.

Thus, knowledge of the state of the ocean is essential for not only studying but also predicting TAV. In particular, subsurface temperature anomalies, in addition to SSTA, are crucial for climate prediction. Our estimate of these crucial variables, as well as their time evolution, is through ocean data assimilation (ODA), which is in principle an optimal estimate of the state of ocean by combining observations with ocean models (Ghil and Malanotte-Rizzoli 1991). Over the past 10–15 years, a number of global ODA systems have been developed to synthesize various observations with the physics described by ocean general circulation models (OGCMs) to estimate the time-evolving, three-dimensional state of ocean circulation. Recently, attention has been focused on the potential differences among these analyses and several studies have been performed to compare and evaluate them in terms of a large suite of indices and variables. For example, Carton and Santorelli (2009) examined the consistency of the temporal variation of global heat content in nine ODA products. Gemmell et al. (2009) evaluated water-mass characteristics of a suite of ODA products against hydrographical measurements. Lee et al. (2009) and Stammer et al. (2010) provide a summary of results of intercomparison of ocean reanalysis carried out by the CLIVAR-GSOP community. Lee et al. (2010) compared the total volume transport of the Indonesian throughflow estimated by 14 global ODA products. Xue et al. (2011a) also performed a comparative analysis of the global upper ocean heat content variability in ten operational ocean analysis, including eight ODA products. Corre et al. (2010) use an ensemble of ocean reanalysis for an attribution study, using fingerprints techniques. These comparisons generally reveal substantial differences among ODA products.

Current ocean reanalysis systems seem to have large uncertainties in estimating subsurface conditions. In the tropics, this problem may be especially serious in the Atlantic basin, where the differences among state-of-the-art ocean reanalysis products are comparable to or even larger than the interannual variability derived from each of these analyses. We use the averaged temperature anomalies in the upper 300 m, an index of the upper ocean heat content anomalies (HCA), as an example. Following Lee et al. (2009), we use the ensemble average from a group of analyses to represent the magnitude of its interannual variability, the deviations of each analysis from this ensemble mean can be used to quantify the level of its uncertainty. Based on this measure, the so-called signal/

noise ratio in the tropical Atlantic Ocean is not only way below that in the equatorial Pacific but also significantly lower than in the tropical Indian Ocean. The ratio is even lower than in some parts of high latitude regions, such as the North Atlantic (Fig. 1). This is consistent with the results reported in Fig. 2 of Lee et al. (2009). The large inconsistency among ocean analyses over the tropical Atlantic brings up some fundamental questions for studying the climate variability in this region. For example, how realistic is the characteristics of TAV derived from one of these reanalysis products? How can we use analyses with this level of uncertainty to explain the physical processes of the TAV? Furthermore, how much can we trust the predictions of TAV with dynamical forecast systems initialized from these analyses (Stockdale et al. 2006; Hu and Huang 2007)?

In general, several factors may contribute to the differences in these analyses. First, different ocean models may be applied to generate first guesses for the analyses. Second, these ocean models may be forced by different atmospheric fluxes, and finally, different assimilation techniques may be used to assimilate slightly different datasets of ocean observations (e.g., Table 1). As a result, the produced ocean analyses contain not only some common signals, which are likely the assimilated observational signals, but also some differences, which may arise from these different sources. Our preliminary analysis suggests that these differences among the analyses are not mainly because one or two analyses are outliers or have larger errors. Instead, it is more likely that uncertainties in the current ODA systems, arising from the factors mentioned above (ocean model, observations, forcing fluxes, assimilation method) cannot be sufficiently reduced by the insertion of observations. In what follows, we refer to this uncertainty as noise. It is important to notice that the nature of this noise is due to uncertainties in the methodology rather than to the intrinsic chaotic nature of the ocean system. For instance, Balmaseda and Weaver (2006) show that a large part of the uncertainty comes from the forcing fluxes and data assimilation methodology. It is still not clear why the level of noise is larger in the tropical Atlantic than in other basins. It is possible that the climate signal in the tropical Atlantic is not as overwhelming as in the tropical Pacific. As such, even with the same noise level in an ocean analysis, the realistic climate signal will be less discernible in the tropical Atlantic than in the tropical Pacific. It is also possible that the physical processes are more complicated in this area due to the confluence of the gyre circulation, equatorial wave dynamics, and deep overturning. In particular, the deep-ocean processes are not strongly constrained by the insertion of the mostly upper ocean observations.

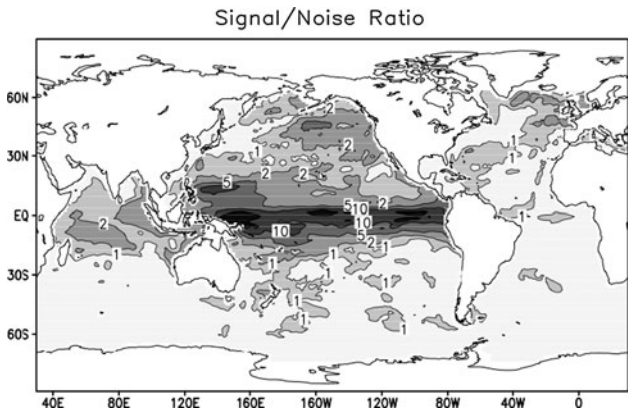

Fig. 1 The global map of the signal versus noise ratio of the upper 300 m mean ocean temperature (HC) for 1979–2007 derived from six ocean reanalysis datasets (i.e., EC ORA-S3, EC COMBINE-NV, NCEP GODAS, NCEP CFSR, UM/TAMU SODA, GFDL ECDA). Contours *1*, *2*, *5*, *10*, *15* are shown. Here signal is defined as the interannual variance in the ensemble mean dataset of six datasets; noise is defined as the variance of the difference between six datasets and their ensemble mean

In this paper, we address the following question: Given the level of uncertainty, how can we get reliable information of the anomalous oceanic variations from the ocean analyses in the tropical Atlantic region? We will present an "ensemble" method to extract the signals in the tropical Atlantic based on multiple-ocean reanalysis products. The underlying assumption for this method is that there exists the realistic climate variability as the common signals among these analyses, but the noise inherent within each dataset should be independent among analyses, as discussed above. An "ensemble" average may reduce the level of independent noise and thus amplify signal-to-noise ratio. In this study, our analysis will be focused on the upper ocean heat content (hereafter refers to as HC, defined as the average temperature of the upper 300 meters). We realize that the HC derived from different analyses may have systematic differences because of their different vertical resolutions. To alleviate this problem, special care has been taken to integrate the temperature to 300 m exactly. Moreover, our analysis is concentrated on the HC anomalies, which is dependent upon the temperature anomalies and less affected by the resolution-induced biases.

The paper is arranged as follows. Six ocean reanalysis products, some validation datasets and our analysis methods are described in Sect. 2. Section 3 presents the results from empirical orthogonal function (EOF) analysis of each individual dataset. Our major results are presented in Sect. 4. An EOF analysis of the ensemble dataset based on the six products is first shown, which is then compared with the ensemble modes extracted by a more sophisticated EOF technique that maximizes the signal-to-noise ratio (MSN EOF hereafter). Also in this section, the advantages of the "ensemble" method are further validated against

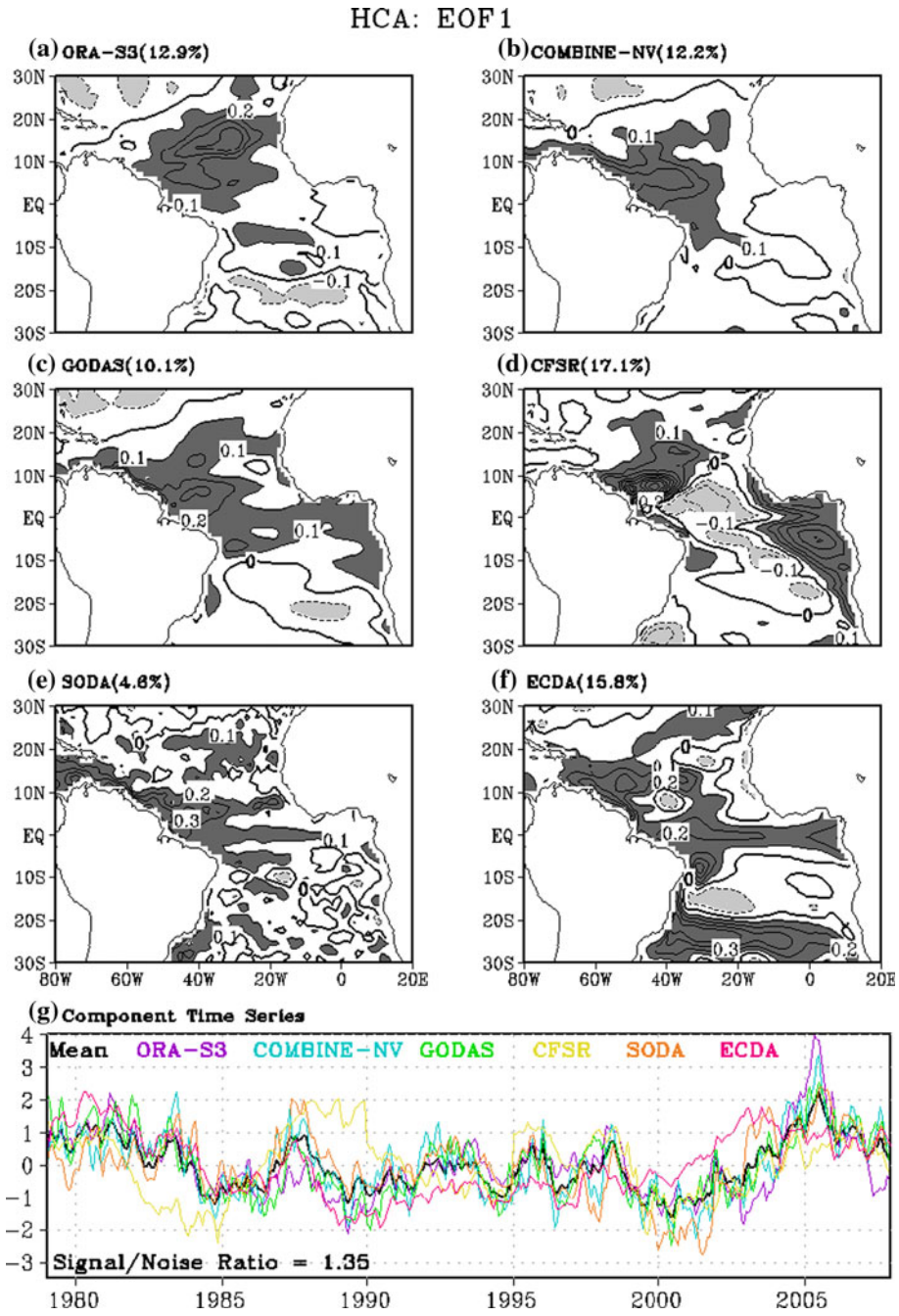

Fig. 2 The first EOF modes of HC anomalies in the tropical Atlantic for 1979–2007 from the product **a** ORA-S3, **b** COMBINE-NV, **c** GODAS, **d** CFSR, **e** SODA, and **f** ECDA. Their corresponding time series are presented in (**g**), with their mean shown as *black curve*. The contour interval in (**a**)–(**f**) is 0.1°C with regions greater than 0.1°C *darkly shaded* and less than −0.1°C have *lightly shaded*

some independent observational datasets including the satellite altimetry data and the mooring station data. The summary and discussion are given in Sect. 5.

2 Datasets and analysis methods

2.1 Six ocean reanalysis products

In this work, our analysis will focus on the tropical Atlantic Ocean. We examined six state-of-the-art global ocean reanalysis products, all of which are widely used in the climate research community. Four of them are from two operational forecast centers, i.e., National Center for Environmental Prediction (NCEP) and European Center for Medium-Range Weather Forecasts (ECMWF), which include their current operational analyses that initialize the operational climate forecasts and the new reanalysis using a more updated analysis system. In the ECMWF, the new analysis system is based on NEMOVAR (Mogensen et al. 2009, Balmaseda et al. 2010). For convenience, the six products are referred to as ORA-S3, COMBINE-NV,

Table 1 Brief summary of ocean state estimation systems

System and institution (reference)	Model and resolution	Method	Data	Period
ORA-S3, ECMWF, EU (Balmaseda et al. 2008)	HOPE 1X(0.3–1), 29 levels	3D OI with online bias correction	Altimeter (sea level anomalies and global trends), SST, T & S from XBT, CTD, Argo, TAO	1959–2009
COMBINE-NV ECMWF, EU (Balmaseda et al. 2010)	NEMO 1X(0.3–1) 42 levels	3D-VAR	EN3_v2a data set (including ocean station/CTD, XBT, Buoys, profilers inWOD05, GTSPP and ARGO)	1958–2008
GODAS, NCEP, USA (Behringer 2005)	MOM3 1X(0.3–1) 40 levels	3D-VAR	SST, T profiles from XBT, CTD, Argo, TAO	1979–2009
CFSR, NCEP, USA (Saha et al. 2010)	NCEP CFS2 (MOM4 0.5X(0.25–0.5) 40 levels)	Partially coupled data assimilation (3D-VAR for OM)	SST, T &S profiles from XBT, CTD, Argo, TAO	1979–2009
SODA 2.1.6, UM/ TAMU, USA (Carton and Giese 2008)	POP 0.25X0.4, 40 levels	OI	Altimetry, satellite and in situ SST, T & S profiles from MBT, XBT, CTD, Argo and other float data, TAO and other buoys.	1958–2008
ECDA, GFDL, USA (Zhang et al. 2007)	GFDL CM2 (MOM4 1X(0.3–1), 50 levels)	Coupled data assimilation (ensemble kalman filter)	SST, T profiles from XBT, CTD, ARGO, TAO & S profiles from CTD, ARGO	1979–2007

GODAS, CFSR, SODA and ECDA, respectively. Both ORA-S3 and COMBINE-NV are from ECMWF. ORA-S3 has been operational since August 2006, providing ocean initial conditions for the ECMWF seasonal and monthly forecasts since March 2007. It is based on the Hamburg Ocean Primitive Equation (HOPE) model (1° with 0.3° equatorial refinement and 29 levels), and 3D Optimal Interpolation (OI) scheme to assimilate temperature, salinity, altimeter derived sea-level anomalies and global sea level trends (Balmaseda et al. 2008). COMBINE-NV is a new ocean reanalysis which assimilates temperature and salinity (not sea level anomalies) using NEMOVAR, a variational data assimilation system based on the NEMO ocean model at ECMWF. More precisely, COMBINE-NV in this paper represents the NEMOVAR-COMBINE ocean reanalysis (Balmaseda et al. 2010), which is slightly different from the ECMWF S4 operational ocean reanalysis system (NEMOVAR-ORAS4). NEMOVAR-COMBINE is delivered for the FP7 COMBINE project (http://www.combine-project.eu/), and will be used for initialization of decadal forecasts by the EC-EARTH consortium. The ocean model has a resolution of 1° with an equatorial refinement to 0.3° in meridional direction, and 42 vertical levels. Both GODAS and CFSR were developed at NCEP. GODAS is based on the Geophysical Fluid Dynamics Laboratory's Modular Ocean Model version 3 (MOM3) at 1° with an equatorial refinement to 0.3° in meridional direction, and 40 vertical levels and a 3D variation scheme (Behringer 2005). CFSR is a partially coupled data assimilation system (Xue et al. 2011b), where the first guess is provided by 6 h coupled model forecasts (Saha et al. 2010). The oceanic model of CFSR is MOM4 with interactive sea-ice, which has a resolution of 0.5° with 0.25° equatorial refinement, and 40 vertical levels. SODA represents Simple Ocean Data Assimilation product, which was generated jointly by University of Maryland and Texas A&M University (Carton and Giese 2008). It is based on optimal interpolation and the Parallel Ocean Program (POP) version 2.1 numerics with 0.25° × 0.4° resolution and 40 vertical levels. In this study, the latest version (i.e., version 2.1.6) of SODA is used. The GFDL ECDA assimilation system consists of an Ensemble Kalman Filter applied to GFDL's second generation fully coupled climate model CM2.1 (Zhang et al. 2007). The ocean component of the ensemble coupled data assimilation system is MOM4 at 1° with 0. 3° equatorial refinement and 50 vertical levels.

Table 1 summarizes the major characteristics of these ocean analyses, including the models, resolutions, assimilation methods, the assimilated data and the available period. In summary, the reanalysis systems involve four different OGCMs: HOPE, NEMO, MOM (version3 or 4), and POP, two of which are employed on a coupled model framework (i.e., for CFSR and ECDA). Most of the models have medium resolutions (0.5°–1°), often with enhanced meridional resolution in the tropics to better resolve the equatorial oceanic waves. For our study, monthly mean fields from these analyses are interpolated to a common 1° × 1° grid. A variety of assimilation methods are used in

different systems, ranging from optimal interpolation (OI) and three-dimensional variational (3D-VAR) methods to the more advanced ensemble Kalman filter (EnKF). The ways by which they are applied ranges from conventionally ocean-alone data assimilation, to partially coupled data assimilation, and to fully coupled data assimilation. The data assimilated into the models include various types of in situ and satellite observations, but there are certain commonalities among them. All the products assimilated in situ temperature-profile data (e.g., from XBT, CTD, Argo, and moorings). However, the sources and the quality-controlled procedures are not necessarily the same. Some of them also assimilate satellite-derived SST, altimeter-based sea surface height (SSH), and salinity profile data from Argo. Detailed descriptions of these products can be found in their respective references. In this paper, our analysis focuses on their commonly available period, i.e., 1979–2007, covering 29 years.

2.2 Validation datasets

The first validation dataset is the altimetry sea level anomaly (SLA), which indirectly represents the variability of upper-ocean heat content in the tropical oceans (Rebert et al. 1985). The SLA maps are from the AVISO project (http://www.aviso.oceanobs.com/en/data/products/sea-surface-height-products/global/msla/index.html#c5122). The gridded SLA fields at 1/3-degree resolution were calculated by combining TOPEX/Poseidon (T/P) and ERS altimeter data, and interpolation between tracks according to the method described by Le Traon et al. (1998), which minimizes the along-track ERS and T/P dual crossover differences and takes long wavelength errors into account. The uncertainty of the SLA products can be decreased to 3 cm on average because of an efficient correction of along-track orbit errors. In this study, the monthly data from December 1992 to December 2007 are used.

The second validation dataset is from the Pilot Research Moored Array in the Tropical Atlantic (PIRATA) project (Servain et al. 1998; http://www.pmel.noaa.gov/tao/disdel/disdel.html). The HC fields derived from the PIRATA subsurface temperature data are used to validate the HC variability in ocean assimilation products directly. In PIRATA project, only a few moorings with less missing values can extend back to 1998. In this study, five moorings with most available data, located at (38°W, 15°N), (38°W, 8°N), (35°W, 0), (23°W, 0) and (10°W, 10°S), are chosen for the validation. The original daily PIRATA temperature data are firstly used to calculate their monthly mean, and then to derive HC anomalies. Considering that there are some missing values in the PIRATA vertical temperature profiles at various levels, the derived HC anomalies from PIRATA are defined as the vertical average of the temperature anomalies within the upper 300 meters. This is slightly different from the procedure applied to the temperature fields with no missing values, like in the case of model outputs or assimilation products, where the ocean temperature is first averaged vertically to get total HC and then its climatology is removed to derive the HCA. The switch of order for the PIRATA data avoids the calculation of the total HC because it can be biased due to the missing temperature data at some levels.

In addition, OI SST (Reynolds et al. 2002) and wind stress for the NCEP/DOE AMIP-II reanalysis (Kanamitsu et al. 2002) are also used to derive the associated patterns with the dominant modes in HC.

2.3 Methods of analysis

In this study, the conventional EOF is used to derive the dominant modes of HC anomalies in each assimilation product and their "ensemble mean" dataset. We will argue that the leading EOF modes from the ensemble mean are more representative of the variability in the tropical Atlantic Ocean. Since six ocean analyses do not form a sufficiently large ensemble, it is possible that the ensemble mean still contains a certain level of noise. To further improve the signal-to-noise ratio and to extract their common signals (also referred to as ensemble modes in this study), the MSN EOF is applied to them. This method was developed by Allen and Smith (1997) and has been used by Venzke et al. (1999), Sutton et al. (2000), Chang et al. (2000), and Huang (2004) in extracting the dominant MSN EOF patterns in ensemble GCM integrations, and by Hu and Huang (2007) in extracting most predictable pattern of the tropical Atlantic in ensemble hindcasts. It deals with the fact that in a moderate ensemble size, an ensemble mean is supposedly composed of a signal and a random part. This approach is to derive patterns that optimize the signal-to-noise ratio from all ensemble members. In our case, the signal part is associated with the interannual (or longer) variance in reality, which shows certain consistency among different reanalysis products due to similar ocean datasets assimilated into them. The noise part is inherent in each individual product, which is associated with the errors in different atmospheric forcing, different ocean models, different assimilation schemes, and so on. In this work, we analyze the first two leading MSN EOF modes and compare them with the conventional EOF analysis of their ensemble mean. Details of MSN EOF are documented by Allen and Smith (1997), Venzke et al. (1999), and Huang (2004).

In addition, linear regression is frequently used to extract the patterns associated with a pre-defined time series or the time series associated with a specific spatial

mode. Correlation is sometimes calculated to examine the consistency in time among different datasets.

3 EOF analysis of individual product

The conventional EOF analysis is conducted for each reanalysis product to derive the dominant modes of their HC variability. Here the first two leading modes are discussed. Figure 2 presents the first EOF spatial patterns and the associated time series, which account for about 12.9% of the total variance in ORA-S3, 12.2% in COMBINE-NV, 10.1% in GODAS, 17.1% in CFSR, 4.6% in SODA, and 15.8% in ECDA, respectively. A first glance of Fig. 2a–f gives the impression that these patterns are quite diverse among each other. At a closer look, the spatial patterns in ORA-S3 (Fig. 2a), COMBINE-NV (Fig. 2b) and GODAS (Fig. 2c) bear more resemblance than those in the other three products. In general, all patterns show basin-wide HC anomalies with a high anomalous HC (warm water) north of 10°S, which seem to extend in two directions, i.e., northeastward to the North African coast and southeastward along South America's northeastern coast to the equator or further south. But the details are quite different among them. In ORA-S3 (Fig. 2a), the core of high HC resides in the central ocean with a clear northeastward extension, while in COMBINE-NV (Fig. 2b) and GODAS (Fig. 2c), the HC cores are located in the western ocean and extend mostly southeastward. Among the first three analyses, the high HC in the northern tropical ocean extends into the eastern Atlantic along the equatorial waveguide in GODAS (Fig. 2c), but not in the other two. However, this equatorial extension is seen in SODA (Fig. 2f) and ECDA (Fig. 2f), where high HC also appear in the off-equatorial western ocean. The northern HC anomalies in ORA-S3 (Fig. 2a), COMBINE-NV (Fig. 2b) and GODAS (Fig. 2c), as well as their major extensions, are also discernable to a certain extent in CFSR (Fig. 2d), SODA (Fig. 2f) and ECDA (Fig. 2g), although they are seriously obscured by the variations intrinsic to these analyses. In some analyses, these internal fluctuations can be quite dominant. For instance, in CFSR (Fig. 2d), the HC spatial pattern is characterized by well-organized negative HC anomalies in the central basin, which extend from the north to south in the central tropical ocean. As a result, the EOF pattern shows a unique positive–negative-positive structure from northwest to southeast. In ECDA, a belt of positive anomalous HC is evident in southern subtropical ocean, covering the whole bands of $\sim$25°S. In comparison with others, the spatial pattern from SODA (Fig. 2e) shows more abundant small-scale features, probably due to the higher resolution of its ocean model. Correspondingly, the explained variance (4.6%) by this mode is much lower than those by the other five products. Although there are major discrepancies in spatial structure, the time series (Fig. 2g) associated with their respective first mode seem to be more consistent with each other, especially on low-frequency variations. The ratio of signal versus noise can reach 1.35, suggesting that the level of the difference among them is lower than that of the interannual/decadal variations in their ensemble mean time series.

The second modes from ORA-S3, COMBINE-NV, GODAS, CFSR, SODA, and ECDA explain about 7.7, 7.9, 7.5, 9.5, 3.3, and 7.5% of their total variances, respectively. The spatial patterns of this mode (Fig. 3) look more consistent than those in the first mode (Fig. 2). Their spatial structures largely represent the subsurface variability related to the Atlantic Niño (Carton and Huang 1994; Huang et al. 1995; Huang and Shukla 1997). In particular, they are characterized by warm HC anomalies in the eastern equatorial basin and off-equatorial cold anomalies in the western Atlantic, demonstrating the out-of-phase displacement of the thermocline depth between the east and west at the peak of warm events in the Gulf of Guinea. In CFSR (Fig. 3d) and ECDA (Fig. 3f), there are some variations polewards of 10°N and 10°S, which are not apparent in the other four products. Similar to the fist mode, SODA shows more abundant small-scale noise and explains lower variance. Their corresponding time series (Fig. 3g) represent higher frequency variations than those associated with the first mode (Fig. 2g). Although there is better coherence in the second mode, the consistency of its EOF time series among the ensemble members is lower than among that for the first mode, based on the measure of the signal/noise ratio (0.96). Moreover, the level of noise is comparable and even larger than the variations in their ensemble mean.

To identify the attribution for the differences is not a trivial task, and at this stage only some suggestions can be put forward. The reanalysis products, whose dominant modes differ the most significantly from the ensemble mean (see next section), are ECDA, CFSR (differences in spatial structure) and SODA (lower value of explained variance). The large differences in the EOF structures of ECDA with respect to those of the ensemble mean could arise from the different wind forcing, since ECDA is the reanalysis that uses a fully coupled data assimilation system, and it is expected for the surface forcing to differ significant from the other products which use the surface forcings from atmospheric reanalyses. It can also arise from the fact that it is the only product that uses EnKF, which assimilates observations with covariance structures derived from the model (in fact, the structure of the first EOF of the ECDA has the footprint of the equatorial wave dynamics). The different spatial structure of the CFSR could arise from the fact that the reanalysis was conducted in several parallel streams instead of in a continuous serial

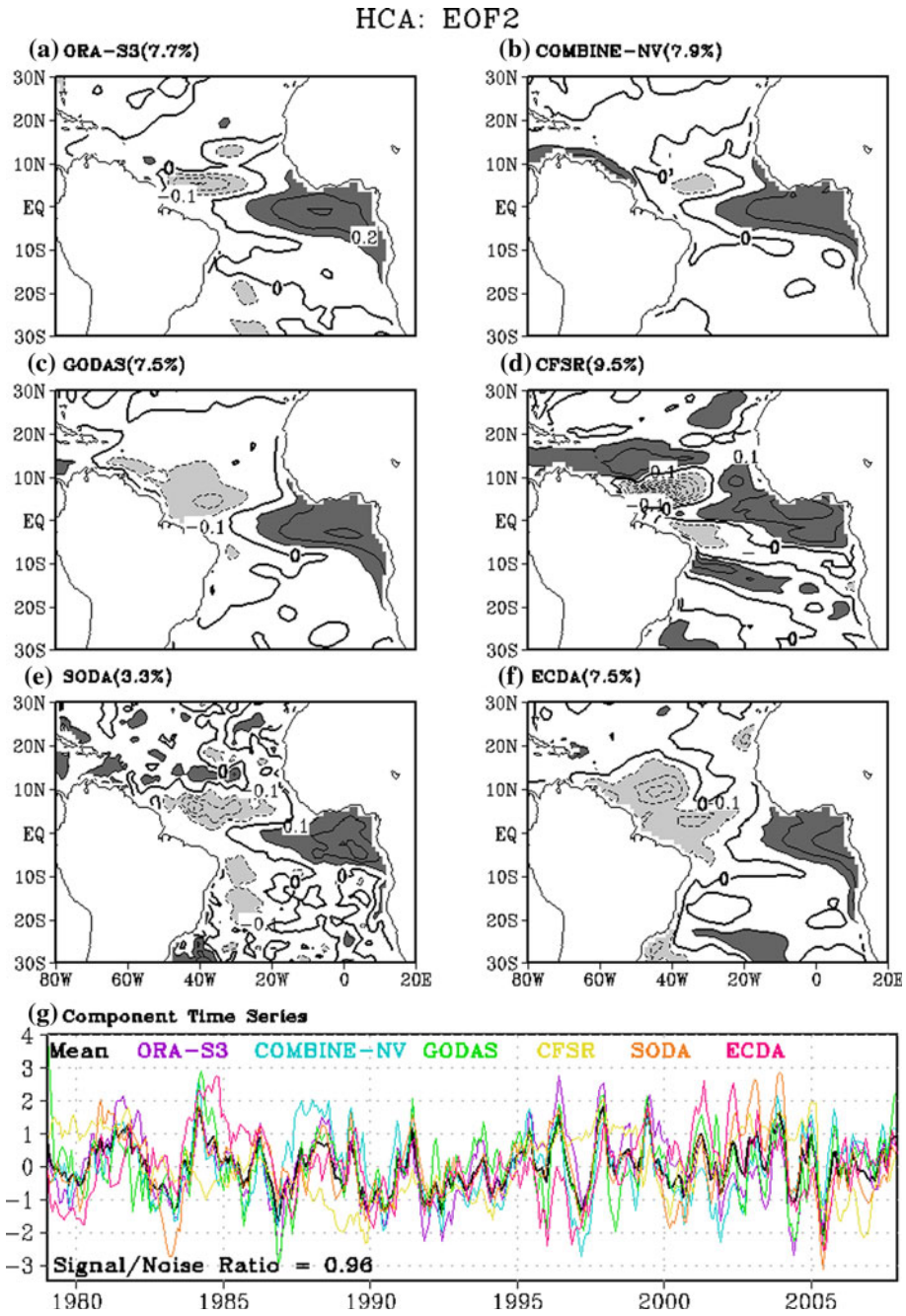

Fig. 3 Same as in Fig. 2, but for the second EOF modes and their corresponding time series

integration (Saha et al. 2010). This approach, widely used in atmospheric reanalyses, may introduce discontinuities in the ocean heat content, causing spurious signals in its interannual variability. The low percentage of explained variance in the SODA reanalysis is consistent with its weak interannual variability, as if a strong constrain to the climatological values were used in this product. But disentangling the origin of the differences among the different reanalysis would only be possible by conducting controlled sensitivity experiments to different aspects of an ocean reanalysis system, such as the input observational data sets, spin-up, forcing fields, ocean model, restoring to climatology (if any), bias correction (if any), specification of background and the observational error covariances, assimilation cycle, and among others, which is beyond the scope of this study.

Overall, our analysis in this section shows that the dominant modes of the HC variability in the tropical Atlantic derived from different ocean analyses show quite diverse features in both their spatial patterns and temporal variations. Although some common features can be traced, they are seriously obscured by the strong internal variations

within each analysis. Further treatment is needed to separate the signals from the noise to get reliable information from these analyses.

4 An ensemble analysis: validation

The analysis in Sect. 3 indicates that even though similar in situ/satellite oceanic datasets have been assimilated into the six reanalysis products, the derived HC changes among them are still noticeably different. Of course, there are more or less consistent signals among them in terms of their leading spatial patterns or time series. Based on the notion that the inconsistent noise among them may be from some (at least partially) independent error sources, an ensemble of them may be a feasible hypothesis to reduce the noise and amplify the signal-to-noise ratio within them. In this paper we will demonstrate that the simple ensemble average is a useful method for this purpose. The ensemble average of these six products will be referred to as the Ensemble Mean (EM) analysis hereafter.

4.1 The EOF modes of the EM analysis

In this subsection, we analyze the HC variability on the interannual and longer time scale in the EM analysis by the conventional EOF. Figure 4a, b show the spatial patterns from the first two leading EOF modes, with their associated time series in Fig. 4c, d as black lines. These two EOF modes account for about 13.7 and 9.0% of the total variance, respectively.

The first mode (Fig. 4a) is characterized by positive basin-wide HC anomalies occupying almost all regions north of 10°S and small negative anomalies around 20°S and north of 20°N. In particular, a high anomalous HC (warm water) appears in the central and western northern tropical Atlantic, and extends northeastward to the North African coast. There also seems to be another extension southeastward to the equator and then towards the eastern Atlantic along the equator (Fig. 4a). The second direction may potentially involve some interaction with the second mode, i.e., Atlantic Niño. This HC pattern is similar to a leading pattern of the HC variability derived by Huang and Shukla (1997) in an ocean simulation forced with observed wind. Ruiz-Barradas et al. (2000) also show a combined rotated EOF mode of both oceanic and atmospheric fields as representing the Atlantic meridional mode. The corresponding HC pattern (See their Fig. 2a) bears certain resemblance to Fig. 4a with the center in the northwestern tropical Atlantic Ocean.

As identified in Huang and Shukla (1997), the distribution of HC anomalies may be associated with a pattern of simultaneously weaker northeast and strong southeast trade winds (see also Fig. 5a). In the western ocean to the north of the equator, the HC anomalies appear to be related to the Ekman pumping induced by simultaneous changes of the northeast and southeast trades, as well as its subsequent effects on the thermocline depths. The associated time series (black line in Fig. 4c) represents a low-frequency (i.e., decadal) variation. Accompanying this mode (derived by regression onto PC1, i.e., black line in Fig. 4c), the SST anomaly field (Fig. 5a) has a well-defined dipole structure, with positive anomalies spreading from the North African coast into the northern ocean and negative anomalies in the south. Therefore, this HC pattern is the subsurface expression of the Atlantic meridional mode.

In the second mode, warm oceanic anomalies appear in the eastern equatorial basin, and cold anomalies appear in the off-equatorial western Atlantic with the northern center more pronounced. The associated time series indicates the mode represents the higher-frequency (i.e., interannual) variability in the tropical Atlantic. Accompanying this mode (derived by regression onto PC2, i.e., black line in Fig. 4d), the SST is characterized by positive anomalies in the mid-eastern equatorial Atlantic, and wind stress weakens to the west of anomalously warm water (Fig. 5b). The variations of the HC, SST and wind stress are consistent with the characteristics of Atlantic Niño (Zebiak 1993; Carton and Huang 1994; Huang and Shukla 1997; Handoh and Bigg 2000; Ruiz-Barradas et al. 2000). In fact, the HC changes in this mode are part of the adjustment by ocean waves due to the fluctuations in the equatorial winds, like ENSO in the tropical Pacific. In particular, when a westerly wind anomaly appears in the western ocean, it generates warm oceanic anomalies propagating eastward as equatorial Kelvin waves, and at the same time produces off-equatorial cold anomalies through the anomalous wind stress curl (Chao and Philander 1993), which tend to propagate westward as Rossby waves. According to its time series (black line in Fig. 4d), several major warm events have occurred during the period of 1979–2007, including 1981, 1984, 1988, 1996, 1997, 1999 and 2003. All these events can be identified from independently constructed observational SST datasets, such as OISST (Reynolds et al. 2002), using the so-called ATL3 index (area averaged SST anomaly over (20°W-0, 3°S-3°N); see Zebiak (1993)).

We have further analyzed whether these EOF modes derived from the EM analysis are representative of the signals contained in the individual analyses. Figure 4c, d show the time series obtained by projecting HC anomalies from six ocean products onto EOF1 (Fig. 4a) and EOF2 (Fig. 4b), respectively. The results are very encouraging. The projected time series from individual analyses are coherent with the principal components of the EOF modes from the EM analysis, both in magnitudes and temporal

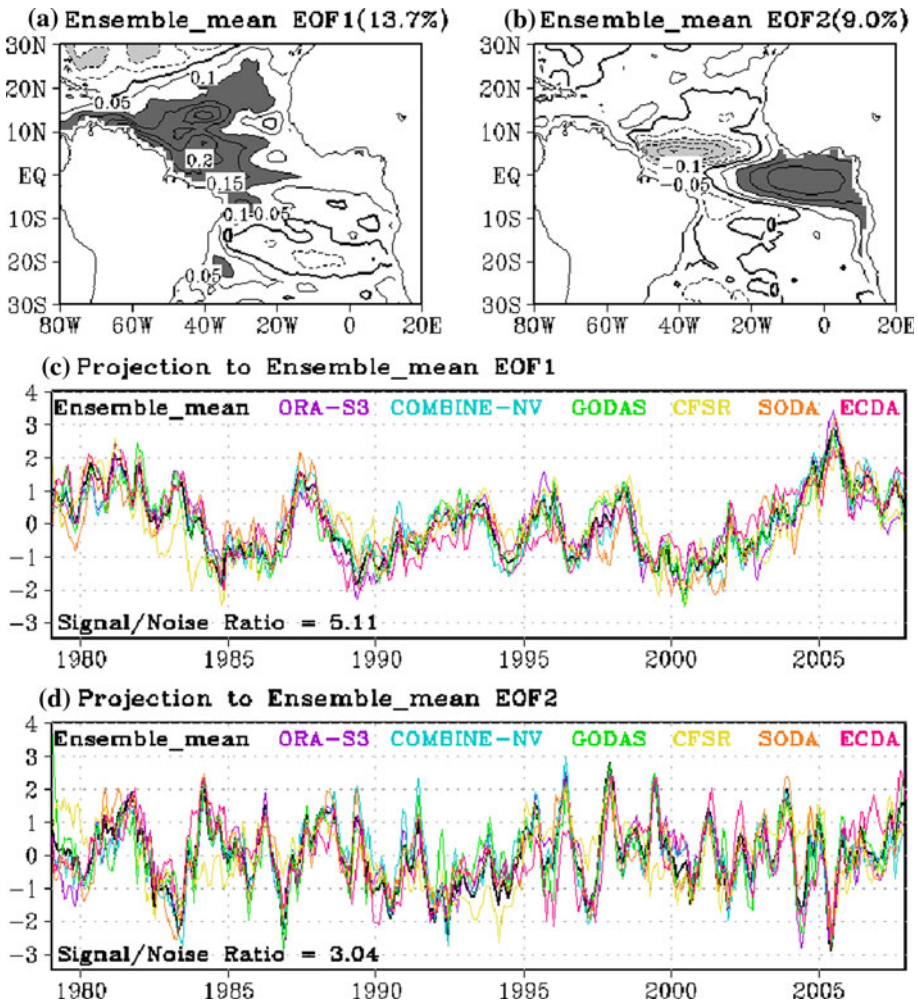

Fig. 4 The **a** first and **b** second EOF modes of HC anomalies in the tropical Atlantic for 1979–2007 from the EM dataset. The contour interval in (**a**)–(**b**) is 0.05°C with regions greater than 0.1°C *darkly shaded* and less than −0.1°C *lightly shaded*. **c** and **d** are the time series of the projection of HC anomalies in the tropical Atlantic from six ocean reanalysis datasets and the EM dataset for 1979–2007 onto (**a**) and (**b**), respectively

variations. Clearly, they are much more strongly correlated among each other than the principal components from their respective leading EOF modes (i.e., Figs. 2g, 3g). Actually, the ratios of the variances of their ensemble mean (signal) and within-ensemble deviations (noise) have significantly increased from 1.35 to 5.11 and 0.96 to 3.04 for the first and second leading modes, respectively. This strongly suggests that the two leading patterns (Fig. 4a, b) from the EM analysis represents the common variability existing in each of the six ocean reanalysis products. Similarly, we also regressed the HC anomalies from each of the ocean analyses onto the two principal components of the two leading EOF modes from the EM analysis. The regressional patterns bear strong resemblance to those shown in Fig. 4a, b. It reinforces our statement that these modes are representative of the common variability in each of these analyses.

4.2 Validation against MSN EOF analysis

In this subsection, we further examine whether the leading EOF modes derived from the EM analysis are adequate, given the fact that six ocean analyses are still a relatively small ensemble. As introduced in Subsect. 2.3, the MSN EOF is theoretically a more sophisticated method to derive ensemble modes by optimizing the ratio of the variances of the ensemble mean and within-ensemble deviations. As such, by performing MSN EOF analysis and comparing with the conventional EOF analysis of our ensemble dataset, it can be examined if our ensemble method (i.e., arithmetic average) can diminish the within-ensemble deviations to a reasonable level.

Figure 6a, b are the first and second MSN EOF modes, with their associated time series shown in Fig. 5c and d as black lines. Comparing with the conventional EOFs from the EM analysis, the explained variances in ensemble mean fields by MSN EOF1 and MSN EOF2 are slightly lower than those by the conventional EOF analysis: 12.8% versus 13.7% and 8.4% versus 9%, respectively. This is consistent with the fact that, by definition, the conventional EOFs explain the maximum amount of the total variance. It may also indicate that the leading modes from the EM analysis may not perfectly represent the most robust ensemble

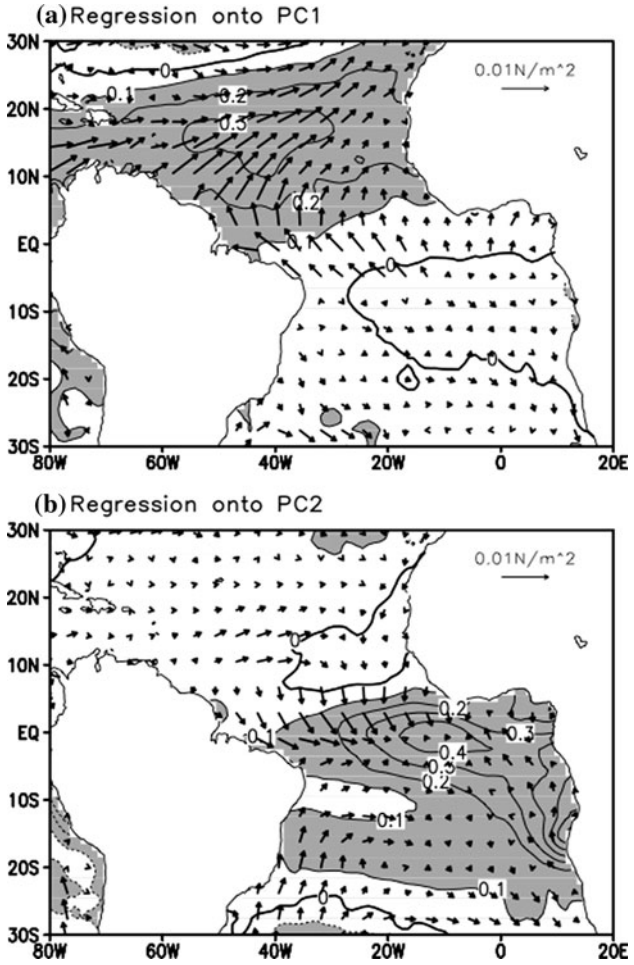

Fig. 5 The regression map of observed SST anomalies and wind stress anomalies onto the **a** first principal component (i.e., *black line* in Fig. 4c) and **b** second principal component (i.e., *black line* in Fig. 4d) of HC anomalies. The regression of SST (wind stress) anomalies is based on November 1981 (December 1979)—December 2007. The contour interval for SST anomalies is 0.1°C. The vector at the bottom of the figure represent 0.01 N/m^2

modes among the six member reanalysis products, due to nonzero noise in the averaged dataset. This is further confirmed by Fig. 6c, d, which show the time series by projecting HC anomalies from six ocean products onto MSN EOF1 (Fig. 6a) and MSN EOF2 (Fig. 6b), respectively. Comparing with their counterparts (Fig. 4c, d) derived by projecting onto the convectional EOF modes, the two groups of time series show similar but slightly more consistent variations among them. The ratios of the variances of their ensemble mean and within-ensemble deviations have slightly increased from 5.11 to 5.25 and 3.04 to 3.54 for the first and second leading modes, respectively. Therefore, the MSN EOFs do show some slight improvements over the conventional EOF modes. On the other hand, considering that the differences, especially in their spatial patterns and time series, are so insignificant, it can be concluded that the noise in the EM analysis has been reduced to a considerably low level. In other words, in our case the simple arithmetic average can generate ensemble fields with noise reduced to an acceptable level. In this sense, the MSN EOF analysis supports the adequacy of the analyses performed in Subsect. 4.1.

4.3 Validation against AVISO sea level dataset

The above two subsections have established that the leading EOF modes from the EM analysis adequately represent the common variability that exists in all six ocean analyses. A further question can be raised on whether they represent the interannual variability in the tropical Atlantic Ocean from 1980 to 2008 more realistically. Until now, there is still no in situ observational HC dataset with basin coverage to validate the derived HC dominant patterns of the tropical Atlantic in individual products (i.e., Figs. 2a–f, 3a–f). On the other hand, previous studies have shown that SLA may be a good representation of the variability of upper-ocean heat content in the tropical ocean (Rebert et al. 1985). Figure 7 gives a quantitative measure of the relationship between SLA and HCA from three analyses, in which the sea level data are available to us. Generally, the correlation between the two variables is significantly high, especially within the equatorial region, where the correlation in GODAS can reach as high as 0.9. Off the equatorial regions, the correlation is not as high, but they are still positively correlated in all three analyses. Therefore, we believe that the altimeter-measured SLA is an adequate indicator of the HCA and the SLA data available since December 1992 is long enough to provide an indirect validation for HC variability.

To validate the spatial patterns of HCA (Figs. 2a–f, 3a–f), the AVISO SL anomaly fields are regressed onto their respective HC principle components of each reanalysis product (Figs. 2g, 3g). The derived SLA patterns are shown in Figs. 8 and 9 for the first and second PCs, respectively. It is interesting to notice that, in contrast with the large difference among the leading HC spatial patterns in six products (Fig. 2a–f), the spatial patterns of AVISO SL anomalies (Fig. 8a–f) associated with their first PCs are more consistent. They more or less represent the fist HC dominant pattern (i.e., Fig. 4a) in the EM analysis. In particular, on the basin scale, the derived SLA are all broadly characterized by positive SL anomalies north of 10°S and small negative anomalies around 20°S. In the northern tropical ocean, there exist two belts of positive SL anomalies, i.e., along 15–20°N and along 5°N, which are generally corresponding to the two extension directions in Fig. 4a. This consistency also proves that the derived HC leading patterns in some oceanic products, like CFSR (i.e., Fig. 2d), may be unrealistic, which is contaminated by

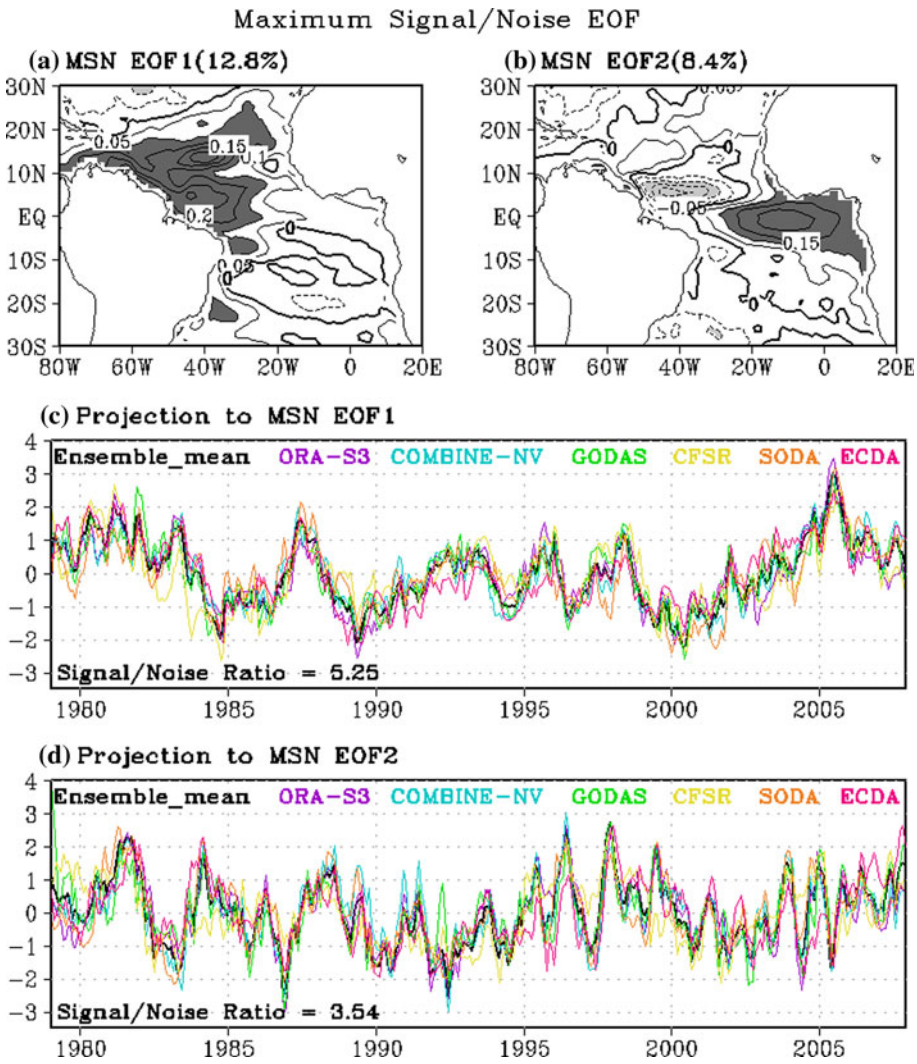

Fig. 6 Same as in Fig. 4, but for MSN EOF analysis

intrinsic noise more seriously than others, possibly because the first guess fields provided by the coupled system contain stronger internal variability that is harder to constrain. Corresponding to the second HC PC of each product, all regression maps (Fig. 9) of AVISO SL anomalies, except for CFSR, well depict the subsurface characteristics of Atlantic Niño, as shown in the second mode of the EM analysis (Fig. 4b). The warm oceanic anomalies appear in the eastern equatorial basin, and cold anomalies appear in the off-equatorial western Atlantic. These characteristics are also shown to a certain extent in the regression map (Fig. 9d) onto CFSR's second PC, but less evident than in others. This should be related to the more distinctive variability in CFSR's second PC. As a whole, the spatial patterns of AVISO SL anomalies and EM HC anomalies (Fig. 8g vs. Fig. 4a and Fig. 9g vs. Fig. 4b) associated with the first two PCs from the EM analysis are more consistent than those respective pairs associated with each reanalysis product. This proves the robustness of the ensemble modes from the EM analysis.

As a more quantitative measure, Fig. 10 calculates the correlations between AVISO SL anomalies and the HC anomalies from six oceanic analyses and the EM analysis. For consistency, in Figs. 10 and 11, all anomalies have been recalculated based on the period of January 1993–December 2007. Generally, the correlations in the tropical Atlantic are significantly lower than those in the tropical Pacific Ocean (the global figures are not shown here; also see Fig. 3 in Stockdale et al. (2006) for the correlation map between the sea levels from altimetry data and those from the ECMWF operational ocean analysis, covering the eastern tropical Pacific and the whole tropical Atlantic), which may need further study to explain. For the tropical Atlantic, all six products generally show higher correlation over the equatorial wave-guide (within 10°N/S) than over other regions (the low correlation off the equatorial regions may partly result from the less correlated property between HCA and SLA; see Fig. 7). But even within the equatorial regions the correlation can reach 0.6 in few of them (mostly $\sim$0.4–0.5). Compared to them, the EM analysis

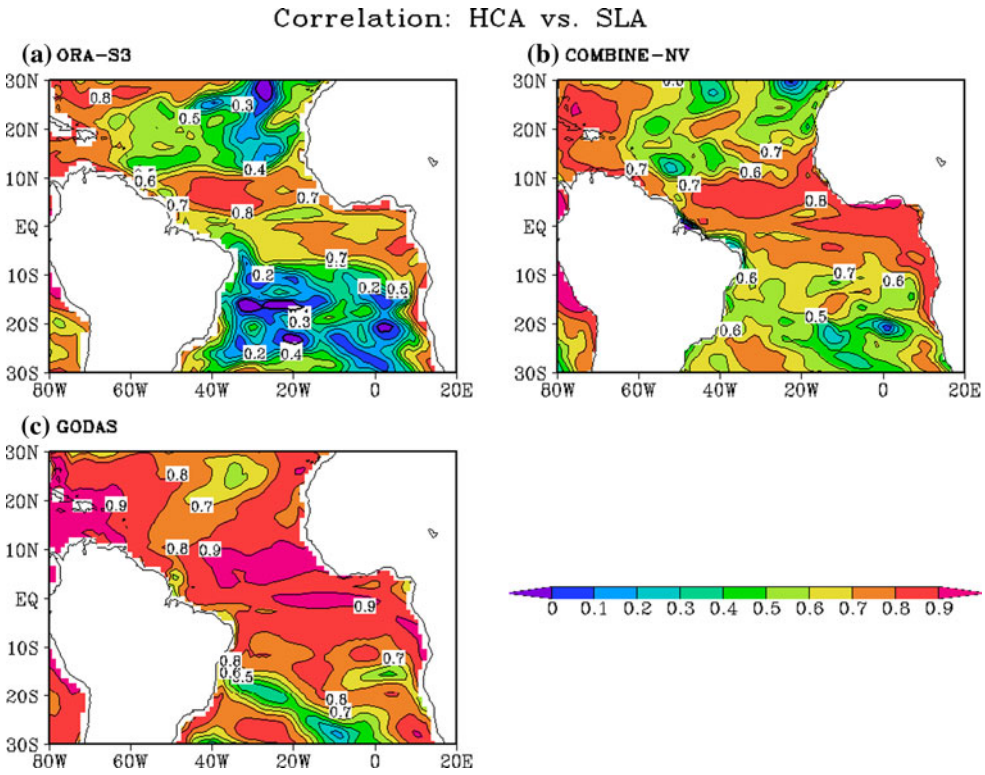

Fig. 7 The correlation map between sea level anomalies and HC anomalies in the tropical Atlantic for January 1979–December 2007 from the product **a** ORA-S3, **b** COMBINE-NV, **c** GODAS

shows higher correlation, with values greater than 0.6 seen over almost all the equatorial belts and values greater than 0.7 over the eastern ocean. In addition, considering the fact that COMBINE-NV seemingly has a competitive correlation comparing with the EM analysis, it is worth checking whether the higher skill around the equator in the EM analysis just originates from the information of COMBINE-NV. To examine this possibility, a five-member (excluding COMBINE-NV) ensemble mean is calculated and compared with the AVISO SL anomalies. As shown by the correlation map (Fig. 10h), the five-member ensemble mean does have a little lower skill around the equator than the all-member ensemble mean, but it is definitely higher than each of the five members, and even higher than COMBINE-NV in the far eastern ocean. This result indicates that the improvement in the EM analysis does not originate from one specific member, but contributed by all members.

In all correlation maps (Fig. 10), there seem to be two regions with higher correlations: eastern equatorial Atlantic and northwestern off-equatorial ocean, which also correspond to two active regions in the HC EOF1 or EOF2 mode (Fig. 4a, b). Figure 11 shows the time series of HC anomalies averaged over the two regions, (45–35°W, 0–10°N) and (10°W-5°E, 6°S-2°N) (referred to as R1 and R2 hereafter), in comparison with AVISO SL anomalies. Over the two regions, all datasets catch the changes of AVISO SL anomalies to some degree. Among the six products, CFSR tends to overestimate the variability, while COMBINE-NV has the highest correlations (0.78 and 0.70 for the two regions, respectively). The use of ERA-Interim forcing fields (Dee et al. 2011) in the COMBINE-NV reanalysis is a likely reason of the higher correlation of the COMBINE-NV (Balmaseda and Mogensen 2010). All six reanalysis products have higher correlations over R1 than over R2. For R1, the correlation in the EM analysis (0.75) is higher than that in five products, but slightly lower than in COMBINE-NV. The improvement over the eastern ocean (i.e., R2) is more significant, where the correlation has increased from 0.50 to 0.70 in six products to 0.78 in the EM analysis.

4.4 Validation against PIRATA mooring dataset

Finally, we compare the HC analyses with those derived from the in situ observations directly. The subsurface temperature data at PIRATA mooring stations can be used to derive HC largely in the same way the analyzed HC is derived. But due to its limited spatial/temporal coverage, the validation like that in Subsect. 4.3 cannot be performed for PIRATA data. Here, only five mooring stations with most available data are picked to compare with the six products and the EM analysis. Although the comparison with PIRATA data does not provide a completely independent verification, since these data have been assimilated in the reanalysis, the anomaly correlation provides a

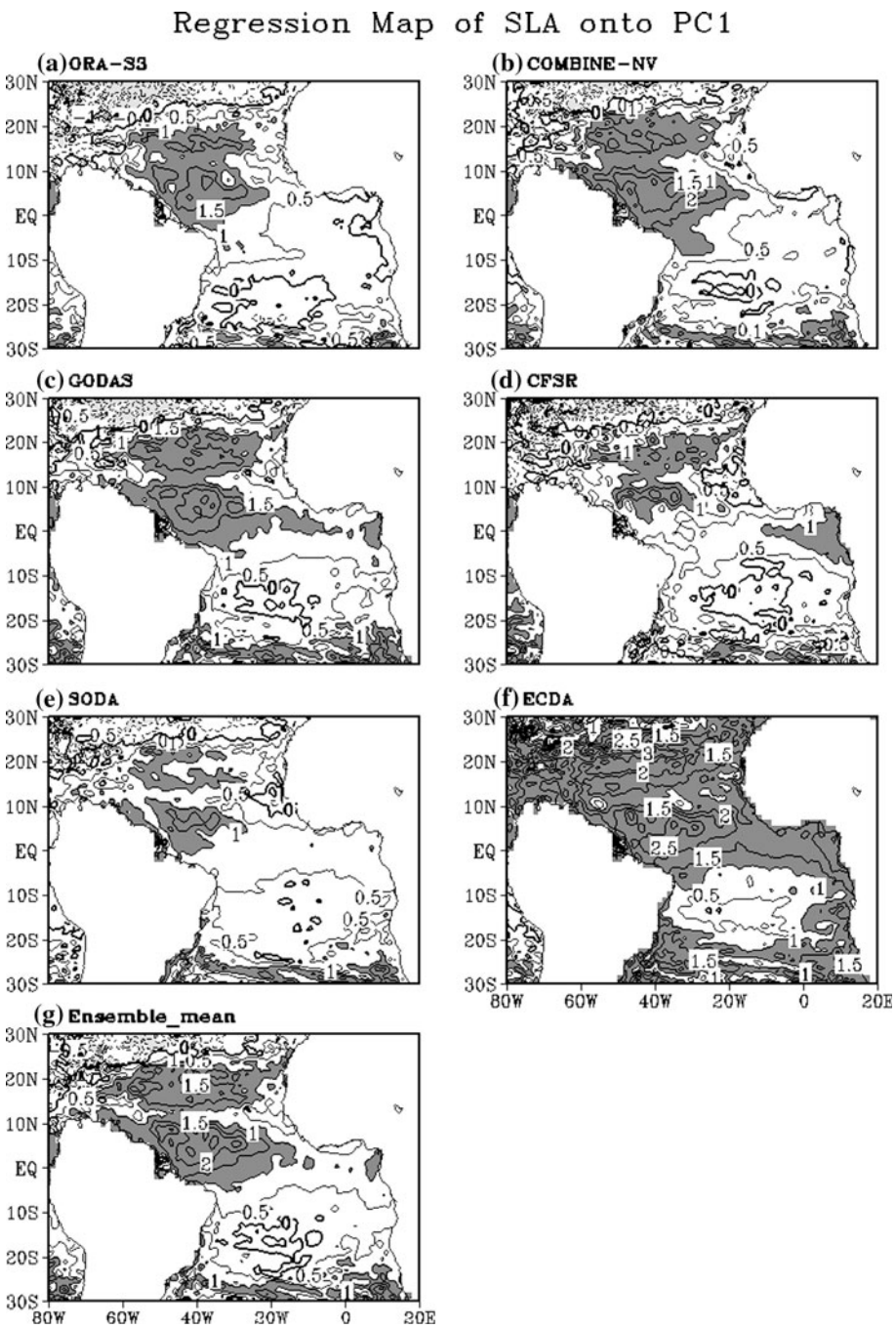

Fig. 8 The regression map of AVISO sea level anomalies onto the first principal components (i.e., Fig. 4c) of HC anomalies for December 1992–2007 from the product **a** ORA-S3, **b** COMBINE-NV, **c** GODAS, **d** CFSR, **e** SODA, **f** ECDA, and **g** the EM dataset. The contour interval in (**a**)–(**g**) is 0.5 cm with regions greater than 1 cm *darkly shaded* and less than −1 cm *lightly shaded*

measure of the ability of the reanalysis to capture the temporal evolution, and it is a powerful diagnostic. For instance, it is possible for a reanalysis to have very low values of root mean square error and low values of the correlation, if too much weight is given to the observations. Figure 12 shows the time series of HC anomalies from PIRATA mooring datasets, six ocean products and the EM analysis at the five stations. For consistency, all anomalies shown in Fig. 12 have been recalculated based on the period of January 1998–December 2007. Their correlations and root mean square deviations (RMSDs) against PIRATA-derived HC anomalies are shown in Tables 2 and 3, respectively. All six products generally capture the observed variability over the five sites with correlations mostly larger than 0.5. Among the six products, COMBINE-NV and GODAS have better skills, while CFSR shows some degree of overestimation again. At the five sites, COMBINE-NV's skill ranges from 0.66 to 0.95 in correlation and 0.12 to 0.32°C in RMSD, and GODAS from 0.82 to 0.94 in correlation and 0.13 to 0.44°C in RMSD. The performance of the EM analysis is better than four products, but sometimes worse than COMBINE-NV

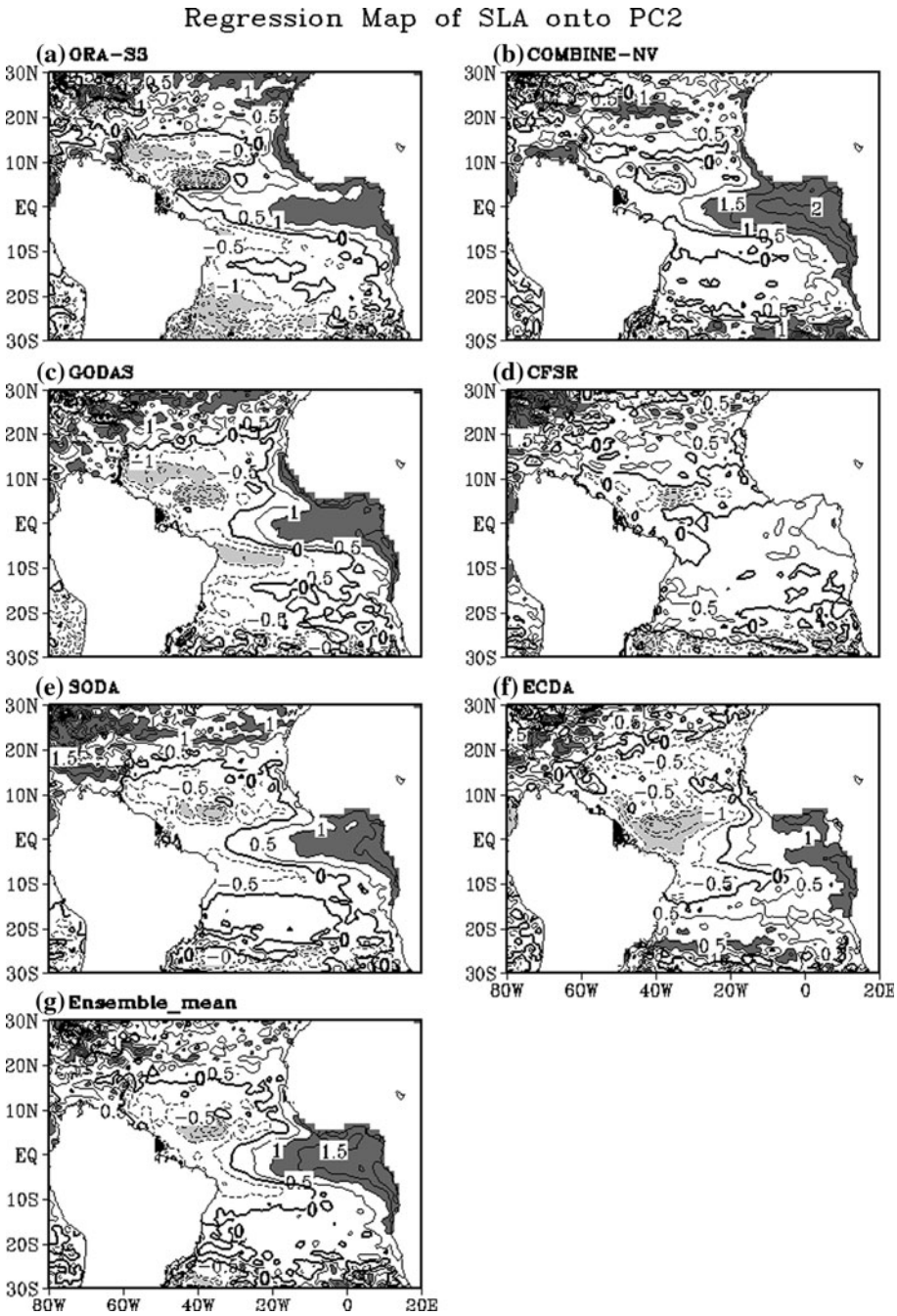

Fig. 9 Same as in Fig. 8, but for the second principal components (i.e., Fig. 4d)

and GODAS, with its skill ranging from 0.74 to 0.91 in correlation and 0.11 to 0.37 in RMSD. In terms of PIRATA-derive HC anomalies, the EM analysis cannot beat COMBINE-NV or GODAS mostly at the off-equatorial stations, like (38 W, 15 N) and (10 W, 10S). In addition, over the five stations, the difference among the six products spread from 0.15°C at (35°W, 0) to 0.36 at (38°W, 8°N). The RMSDs between the EM analysis and PIRATA are now smaller than the ensemble spread at (38°W, 15°N) and (23°W, 0), and larger at (38°W, 15°N) and (35°W, 0). But considering the uncertainty related to the missing values in the PIRATA temperature profiles, the EM analysis generally gets more realistic variability at the five sites.

5 Conclusion and discussion

Nowadays, it is still a major challenge to perform dynamic SST anomalies prediction in the tropical Atlantic on seasonal time scales. In fact, routine SST forecasts in the tropical Atlantic are largely based on statistical approaches (Penland and Matrosova 1998), which are probably at least

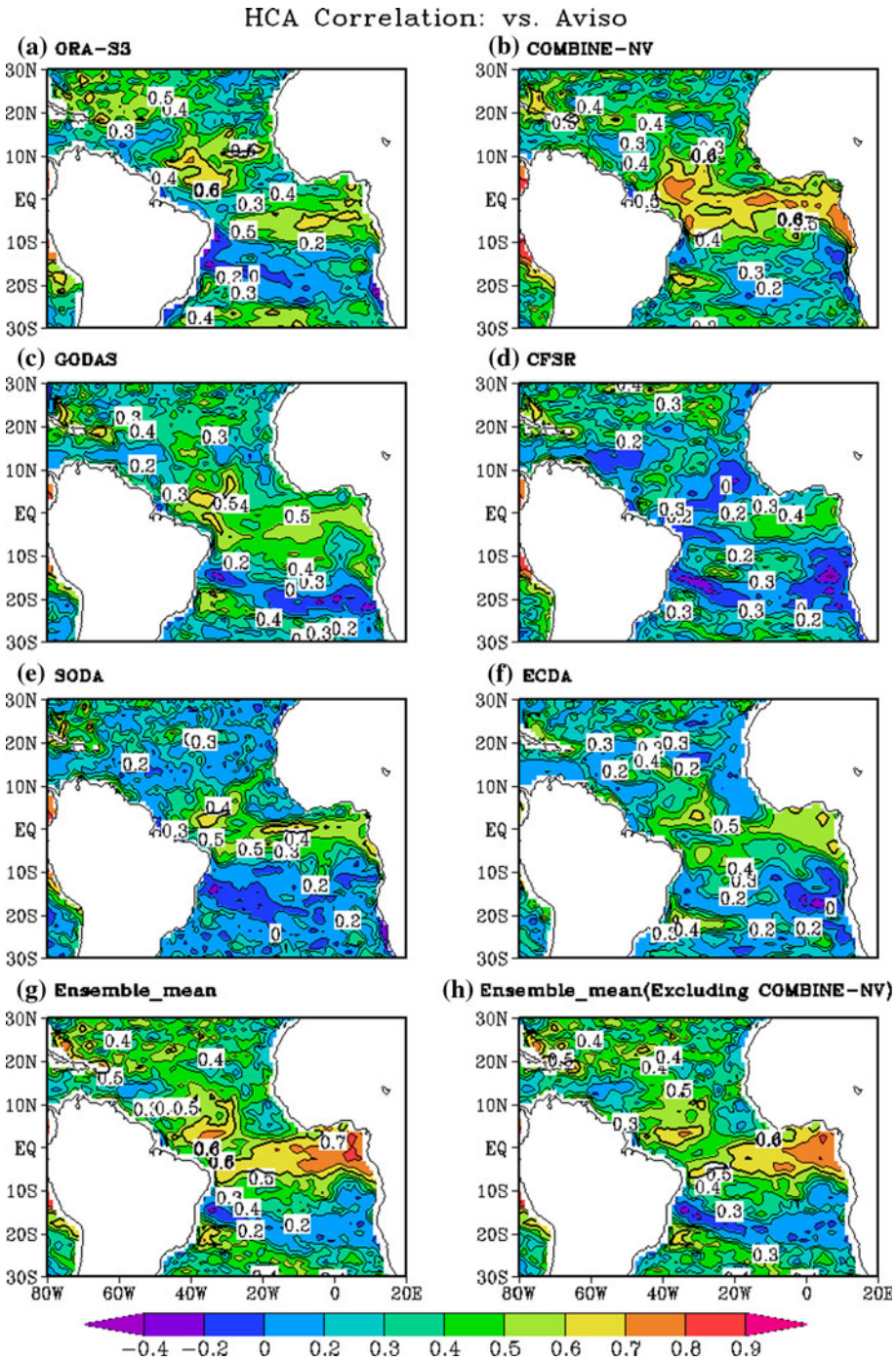

Fig. 10 The correlation map between AVISO sea level anomalies and HC anomalies in the tropical Atlantic for December 1992–2007 from the product **a** ORA-S3, **b** COMBINE-NV, **c** GODAS, **d** CFSR, **e** SODA, **f** ECDA, **g** the EM dataset, and **h** the five-member ensemble mean (excluding COMBINE-NV)

as good as the dynamical predictions. Since these air-sea feedback processes generally have long intrinsic time scales, they should in principle have high climate predictability on seasonal-to-interannual time scales (Kushnir et al. 2006). Therefore, it is puzzling to see that dynamical climate models only show modest skill in the tropical Atlantic compared to ENSO forecast (Chang et al. 1998; Stockdale et al. 2006; Hu and Huang 2007). This problem is generally attributed to two factors, i.e., the biases in dynamical climate models and the uncertainty in the initial states. As for the first factor, it has been recognized that dynamical climate models have significant systematic errors to predict tropical Atlantic SST (e.g., Huang et al. 2007; Richter and Xie 2008; Wahl et al. 2011), which can be a severe obstacle to skillful predictions of tropical Atlantic variability (TAV). The second factor is an issue that has not been fully examined so far. For operational forecasts, the component models are usually initialized from their respective analysis systems (Hu and Huang 2007). For example, ocean models are initialized from

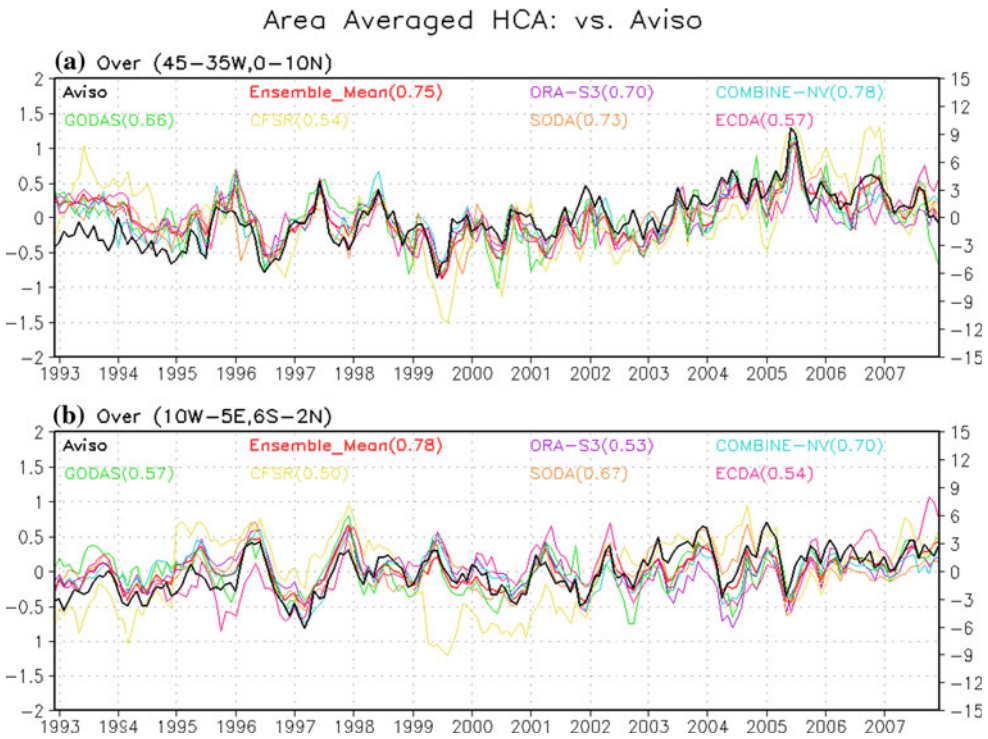

Fig. 11 Time series of area averaged AVISO sea level and HC anomalies for December 1992–2007 from six ocean reanalysis products and the EM dataset over **a** (45–35°W, 0–10°N), and **b** (10°W–5°E, 6°S–2°N). The correlations between sea level anomalies and the respective HC anomalies are shown in *parentheses*

ocean reanalysis systems. However, the current ocean reanalysis systems are far from perfect in estimating the subsurface conditions in the tropical Atlantic Ocean. Our study has shown the difference among the reanalysis datasets is equivalent to or even larger than the interannual variability (Fig. 1). This level of uncertainty in current ocean analyses will have serious consequence to both the mechanism and predictability studies in this area.

In this paper, we presented an "ensemble" method to estimate the variability of upper-ocean heat content in the tropical Atlantic based on multiple-ocean reanalysis products. In particular, our analysis is based on six ocean reanalysis products—ORA-S3, COMBINE-NV, GODAS, CFSR, SODA and ECDA, and their commonly available period from 1979 to 2007. The conventional EOF analysis is firstly conducted on HC fields from the six products. Results indicate that even the dominant modes show significant difference, especially for the first EOF modes, although there exist some common characteristics. For example, the second EOF modes of all six products generally represent the subsurface variability related to the Atlantic Niño. Then, we applied the simple arithmetic average to produce an ensemble dataset, i.e., the EM analysis. The comparison between EOF analysis of the Ensemble Mean dataset and MSN EOF analysis of six products revealed that the ensemble average could generate ensemble fields with noise reduced to an acceptable level in our case. The quality of the EM analysis is further validated against AVISO altimetry SLA data and PIRATA mooring station data. The comparison with AVISO SLA data proved that the leading modes in the EM analysis are realistic, while those in some reanalysis products might be contaminated by intrinsic noises too much. More quantitative correlation analysis indicated the HC fields were improved in the EM analysis, especially over the equatorial regions, with contributions from all ensemble members. The direct comparison with PIRATA-derived HC fields showed that the EM analysis generally gets realistic HC variability at the chosen five mooring stations.

Generally, our results show that there are advantages in using an ensemble of ocean analyses to get more reliable and realistic information on the low-frequency variability in the tropical Atlantic Ocean, considering the large and qualitative differences among different analysis products. In particular, the ensemble mean analysis has been proved to be more realistic, comparing with the individual dataset. The further applications of the dataset in physical process study and prediction study are in progress. In addition, even though arithmetic mean has reduced the noise to a low level, some products, like COMBINE-NV and GODAS, seem to show better quality than others, which can be further exploited by applying non-equal weights to different products to refine our method.

In addition, it is worth noting that the two leading HC modes in the EM analysis are of physical basis and consistent with the major modes of the SST variability derived from many independent sources. The first mode is characterized by positive basin-wide HC anomalies occupying

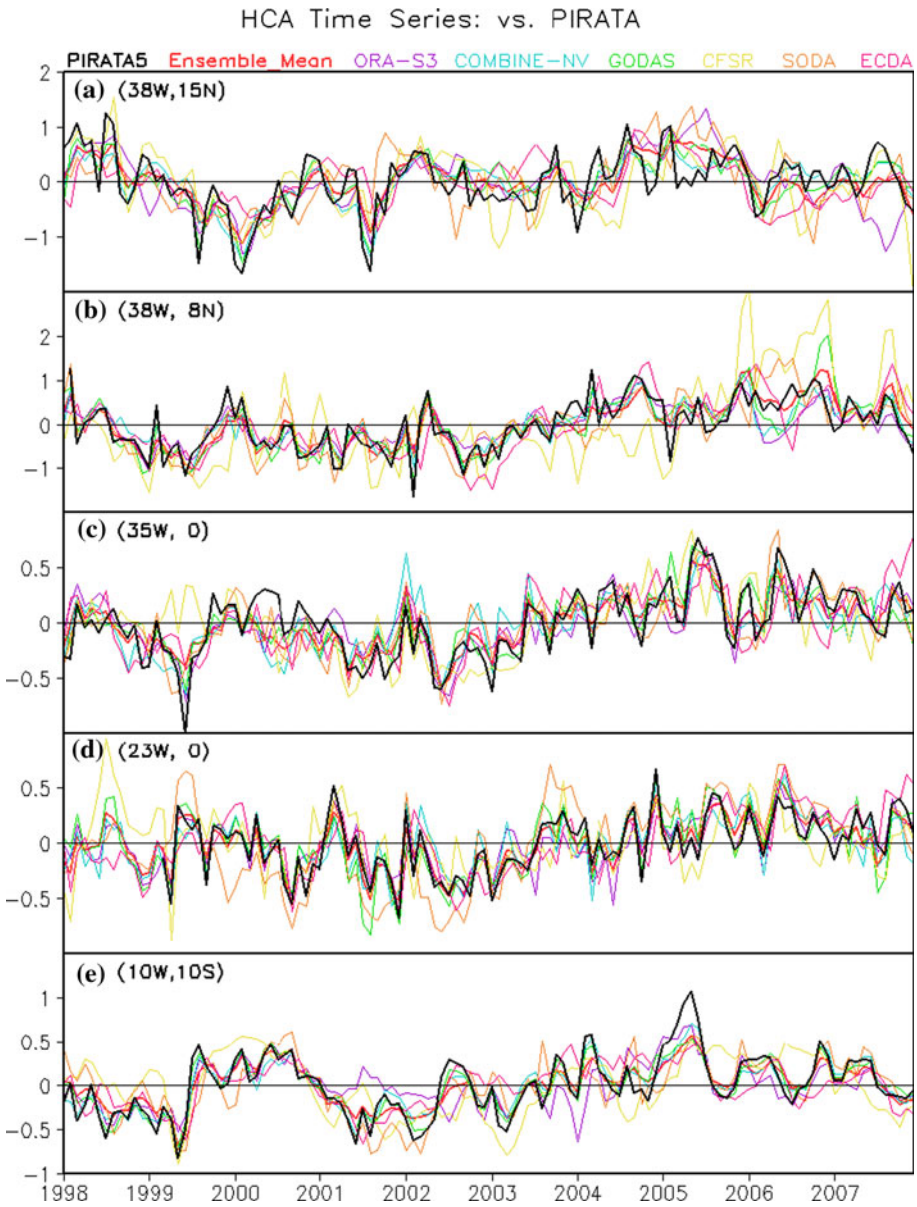

Fig. 12 Time series of HC anomalies for January 1998–2007 from PIRATA 5 mooring data, six ocean reanalysis products and the EM dataset: **a** (38°W, 15°N), **b** (38°W, 8°N), **c** (35°W, 0), **d** (23°W, 0), and **e** (10°W, 10°S)

Table 2 Anomaly correlations between the time series of HC anomalies from PIRATA mooring datasets and those from six ocean products and Ensemble_mean dataset

	Ensemble_Mean	ORA-S3	COMBINE-NV	GODAS	CFSR	SODA	ECDA
(38 W,15 N)	0.74	0.55	**0.81**	**0.83**	0.58	0.47	0.30
(38 W,8 N)	0.82	0.76	**0.86**	0.82	0.49	0.74	0.61
(35 W,0)	0.83	0.77	0.66	**0.84**	0.57	0.72	0.59
(23 W,0)	0.91	0.81	0.78	0.86	0.68	0.72	0.65
(10 W,10S)	0.90	0.71	**0.95**	**0.94**	0.54	0.71	0.64

The correlations lager than those in EM analysis are shown in boldface

almost all regions north of 10°S and small negative anomalies around 20°S and north of 20°N. It is accompanied by a well-defined dipole structure in the SST anomaly fields. Its extension southeastward to the equator may potentially affect the second mode, i.e., Atlantic Niño. Its time series represents a relatively low-frequency (i.e.,

Table 3 Same as Table 2 but for root mean square deviations (RMSDs)

	Ensemble_Mean	ORA-S3	COMBINE-NV	GODAS	CFSR	SODA	ECDA	Ensemble spread
(38 W,15 N)	0.37	0.51	**0.32**	**0.30**	0.53	0.55	0.57	0.29
(38 W,8 N)	0.34	0.38	**0.30**	0.37	0.87	0.44	0.53	0.36
(35 W,0)	0.17	0.20	0.24	0.17	0.28	0.22	0.27	0.15
(23 W,0)	0.11	0.16	0.17	0.15	0.21	0.27	0.23	0.16
(10 W,10S)	0.16	0.24	**0.12**	**0.12**	0.33	0.25	0.26	0.16

The ensemble spread among six ocean products is also shown in the last column. Units are °C. The RMSDs smaller than those in EM analysis are shown in boldface

decadal) variation; in particular, positive during the period of 1979–1983 and 2003–2007, and negative during 1984–1986, 1988–1991, and 1999–2003. The second mode corresponds to Atlantic Niño, characterized by warm oceanic anomalies in the eastern equatorial basin, and cold anomalies in the off-equatorial western Atlantic. The accompanying SST variability is positive anomalies in the mid-eastern equatorial Atlantic. The associated time series represents the interannual variability, such as the warm events of 1981, 1984, 1988, 1996, 1997, 1999 and 2003.

Acknowledgments Funding for this study is provided by the NOAA CVP Program (NA07OAR4310310). The authors would like to thank Drs. J. Shukla and J. Kinter for their guidance and support of this project. We are grateful to two anonymous reviewers for their suggestions and comments. We would also like to thank Dr. V. Krishnamurthy and an anonymous reviewer within COLA for their comments on an earlier version of the manuscript. We thank ECMWF, NCEP, GFDL for providing their ocean data assimilation analysis datasets and Dr. B. Giese for providing the SODA ocean data assimilation analyses. The availability of these datasets makes this analysis possible.

References

Allen MR, Smith LA (1997) Optimal filtering in singular spectrum analysis. Phys Lett 234:419–428

Balmaseda MA, Mogensen K (2010) Evaluation of the ERA-INTERIM forcing fluxes from an ocean perspective. ECMWF ERA report series no. 6. http://www.ecmwf.int/publications/library/do/references/list/782009

Balmaseda MA, Weaver A (2006) Temperature, salinity, and sea level: climate variability from ocean reanalyses. Paper presented at the CLIVAR/GODAE meeting on ocean synthesis evaluation, August 31–September 1, 2006, ECMWF, Reading, UK. Meeting presentation available at: http://www.clivar.org/organization/gsop/synthesis/groups/Items3_4.ppt. Accessed 26 May 2009

Balmaseda M, Vidard A, Anderson D (2008) The ECMWF system 3 ocean analysis system. Mon Wea Rev 136:3018–3034

Balmaseda M, Mogensen K, Molteni F, Weaver A (2010) The NEMOVAR-COMBINE ocean re-analysis. COMBINE technical report no. 1. http://www.combine-project.eu/Technical-Reports.1668.0.html

Behringer DW (2005) The global ocean data assimilation system (GODAS) at NCEP, 11th symposium on integrated observing and assimilation systems for the atmosphere, oceans, and land surface (IOAS-AOLS), San Antonio, TX. Amer Meteor Soc, vol 3.3

Carton JA, Giese BS (2008) A reanalysis of ocean climate using simple ocean data assimilation (SODA). Mon Wea Rev 146:2999–3017

Carton JA, Huang B (1994) Warm events in the tropical Atlantic. J Phys Oceanogr 4:888–903

Carton JA, Santorelli A (2009) Global decadal upper-ocean heat content as viewed in nine analyses. J Clim 21:6015–6035

Chang P, Ji L, Li H (1997) A decadal climate variation in the tropical Atlantic Ocean from thermodynamic air-sea interactions. Nature 385:516–518

Chang P, Ji L, Li H, Penland C, Matrasova L (1998) Prediction of tropical Atlantic sea surface temperature. Geophys Res Lett 25:1193–1196

Chang P, Saravanan R, Ji L, Hegerl GC (2000) The effect of local sea surface temperatures on atmospheric circulation over the tropical Atlantic sector. J Clim 13:2195–2216

Chao Y, Philander SGH (1993) On the structure of the Southern Oscillation. J Clim 6:450–469

Chiang JCH, Bitz CM (2005) Influence of high latitude ice cover on the marine intertropical convergence zone. Clim Dyn 25:477–496. doi:10.1007/s00382-005-0040-5

Corre L, Terray L, Balmaseda M, Ribes A, Weaver A (2010) Can oceanic reanalyses be used to assess recent anthropogenic changes and low-frequency internal variability of upper ocean temperature? Clim Dyn. doi:10.1007/s00382-010-0950-8

Dee D et al (2011) The ERA-interim reanalysis: configuration and performance of the data assimilation system. Accepted by Quart J Roy Meteor Soc

Dong B-W, Sutton RT (2002) Adjustment of the coupled ocean-atmosphere system to a sudden change in the thermohaline circulation. Geophys Res Lett 29(15):1728. doi:10.1029/2002GL015229

Enfield DB, Mayer DA (1997) Atlantic sea surface temperature variability and its relation to El Niño-Southern Oscillation. J Geophys Res 102(C1):929–945. doi:10.1029/96JC03296

Florenchie P, Reason CJC, Lutjeharms JRE, Rouault M, Roy C, Masson S (2004) Evolution of interannual warm and cold events in the southeast Atlantic Ocean. J Clim 17:2318–2334

Folland C, Palmer T, Parker D (1986) Sahel rainfall and worldwide sea surface temperatures. Nature 320:602–606

Gemmell AL, Smith GC, Haines K, Blower JD (2009) Validation of ocean model syntheses against hydrography using a new web application. J Op Oceangr 2(2):29–41

Ghil M, Malanotte-Rizzoli P (1991) Data assimilation in meteorology and oceanography. Adv Geophys 33:141–266

Handoh IC, Bigg GR (2000) A self-sustaining climate mode in the tropical Atlantic, 1995–1997: observations and modelling. Quart J Roy Meteor Soc 126:807–821

Hastenrath S, Heller L (1977) Dynamics of climatic hazards in northeast Brazil. Quart J Roy Meteor Soc 103:77–92
Hirst AC, Hastenrath S (1983) Atmosphere–ocean mechanisms of climate anomalies in the Angola–Tropical Atlantic sector. J Phys Oceanogr 13:1146–1157
Hu Z-Z, Huang B (2007) The predictive skill and the most predictable pattern in the tropical Atlantic: the effect of ENSO. Mon Wea Rev 135:1786–1806
Huang B (2004) Remotely forced variability in the tropical Atlantic Ocean. Climate Dyn 23:133–152
Huang B, Shukla J (1997) Characteristics of the interannual and decadal variability in a general circulation model of the tropical Atlantic Ocean. J Phys Oceanogr 27:1693–1712
Huang B, Shukla J (2005) Ocean–atmosphere interactions in the tropical and subtropical Atlantic Ocean. J Clim 18:1652–1672
Huang B, Carton JA, Shukla J (1995) A numerical simulation of the variability in the tropical Atlantic Ocean, 1980–1988. J Phys Oceanogr 25:835–854
Huang B, Hu Z-Z, Jha B (2007) Evolution of model systematic errors in the tropical Atlantic basin from the NCEP coupled hindcasts. Clim Dyn 28(7/8):661–682. doi:10.1007/s00382-006-0223-8
Joyce TM, Frankignoul C, Yang J, Phillips HE (2004) Ocean response and feedback to the SST dipole in the tropical Atlantic. J Phys Oceanogr 34:2525–2540
Kanamitsu M, Ebisuzaki W, Woollen J, Yang S-K, Hnilo JJ, Fiorino M, Potter GL (2002) NCEP-DOE AMIP-II reanalysis (R-2). Bull Amer Meteor Soc 83:1631–1643
Kushnir Y, Robinson WA, Chang P, Robertson AW (2006) The physical basis for predicting Atlantic sector seasonal-to-interannual climate variability. J Clim 23:5949–5970
Lamb PJ (1978) Large-scale tropical Atlantic surface circulation patterns associated with subsaharan weather anomalies. Tellus 30:240–251
Le Traon PY, Nadal F, Ducet N (1998) An improved mapping method of multi-satellite altimeter data. J. Atmos Oceanic Technol 25:522–534
Lee S-K, Wang C (2008) Tropical Atlantic decadal oscillation and its potential impact on the equatorial atmosphere-ocean dynamics: a simple model study. J Phys Oceanogr 38:193–212
Lee T, Awaji T, Balmaseda MA, Grenier E, Stammer D (2009) Ocean state estimation for climate research. Oceanography 22:160–167
Lee T et al (2010) Consistency and fidelity of Indonesian-throughflow total volume transport estimated by 14 ocean data assimilation products. Dyn Atmos Oceans 50:201–223
Mahajan S, Saravanan R, Chang P (2011) The role of the wind-evaporation-sea surface temperature (WES) feedback as a thermodynamic pathway for the equator-ward propagation of high latitude sea-ice induced cold anomalies. J Clim (in press). doi:10.1175/2010JCLI3455.1
Mogensen K, Balmaseda MA, Weaver AT, Martin M, Vidard A (2009) NEMOVAR: a variational data assimilation system for the NEMO ocean model. ECMWF Newslett 120:17–22
Moura AD, Shukla J (1981) On the dynamics of the droughts in northeast Brazil: observations, theory and numerical experiments with a general circulation model. J Atmos Sci 38:2653–2675
Nobre P, Shukla J (1996) Variations of sea surface temperature, wind stress, and rainfall over the tropical Atlantic and South America. J Clim 9:2464–2479
Penland C, Matrosova L (1998) Prediction of tropical Atlantic sea surface temperatures using linear inverse modeling. J Clim 11:483–496
Rebert JP, Donguy JR, Eldin G, Wyrtki E (1985) Relations between sea level, thermocline depth, heat content, and dynamic height in the tropical Pacific Ocean. J Geophys Res 90:11719–11725
Reynolds RW, Rayner NA, Smith TM, Stokes DC, Wang WQ (2002) An improved in situ and satellite SST analysis for climate, *J*. Climate 15(13):1609–1625
Richter I, Xie S-P (2008) On the origin of equatorial Atlantic biases in coupled general circulation models. Clim. Dyn. 31:587–598
Ruiz-Barradas A, Carton JA, Nigam S (2000) Structure of interannual-to-decadal climate variability in the tropical At- lantic sector. J Clim 13:3285–3297
Saha S et al (2010) The NCEP climate forecast system reanalysis. Bull Am Met Soc 91:1015–1057
Servain J (1991) Simple climatic indices for the tropical Atlantic Ocean and some applications. J Geophys Res 96(C8):15137–15146
Servain J, Picaut J, Merle J (1982) Evidence of remote forcing in the equatorial Atlantic Ocean. J Phys Oceanogr 12:457–463
Servain J, Busalacchi AJ, McPhaden MJ, Moura AD, Reverdin G, Vianna M, Zebiak SE (1998) A pilot research moored array in the tropical atlantic (PIRATA). Bull Am Meteorol Soc 79:2019–2031
Servain J, Wainer I, McCreary JP, Dessier A (1999) Relationship between the Equatorial and meridional modes of cli- matic variability in the tropical Atlantic. Geophys Res Lett 26:485–488
Stammer et al (2010) Ocean information provided through ensemble ocean syntheses. In Hall J, Harrison DE, Stammer D (eds) Proceedings of "OceanObs'09: sustained ocean observations and information for society" conference, vol 2, Venice, Italy, 21–25 September 2009, ESA Publication WPP-306
Stockdale TN, Balmaseda M, Vidard A (2006) Tropical Atlantic SST prediction with coupled ocean–atmosphere GCMs. J Clim 19:6047–6061
Sutton RT, Jewson SP, Rowell DP (2000) The elements of climate variability in the tropical Atlantic region. J Clim 13:3261–3284
Venzke S, Allen MR, Sutton RT, Rowell DP (1999) The atmospheric response over the North Atlantic to decadal changes in sea surface temperature. J Clim 12:2562–2584
Wagner RG, da Silver A (1994) Surface conditions associated with anomalous rainfall in the Guinea coastal region. Int J Climatol 14:179–199
Wahl S, Latif M, Park W, Keenlyside N (2011) On the tropical atlantic SST warm bias in the Kiel climate model. Clim Dyn 36:891–906
Wen C, Chang P, Saravanan R (2009) Effect of atlantic meridional overturning circulation changes on tropical atlantic sea-surface temperature variability: A 2-1/2 layer reduced gravity ocean model study. J Clim. doi:10.1175/2009JCLI3042.1
Xie S-P (1999) A dynamic ocean–atmosphere model of the tropical Atlantic decadal variability. J Clim 12:64–70
Xie S-P, Carton JA (2004) Tropical Atlantic variability: patterns, mechanisms, and impacts. In: Wang C, Xie S-P, Carton JA (eds) Earth's climate: the ocean–atmosphere interaction. Geophysical Monograph, NO. 147, Amer Geophys. Union, Washington DC, pp 121–142
Xue Y et al (2011a) Comparative analysis of upper ocean heat content variability from ensemble operational ocean analysis. U.S. CLIVAR 9(1):7–10
Xue Y, Huang B, Hu Z, Kumar A, Wen C, Behringer D, Nadiga S (2011b) An assessment of oceanic variability in the NCEP climate forecast system reanalysis. Clim Dyn. doi:10.1007/s00382-010-0954-4
Yang JY (1999) A linkage between decadal climate variations in the Labrador Sea and the tropical Atlantic Ocean. Geophys Res Lett 26:1023–1026
Zebiak SE (1993) Air–sea interaction in the equatorial Atlantic region. J Clim 8:1567–1586
Zhang S, Harrison MJ, Rosati A, Wittenberg A (2007) System design and evaluation of coupled ensemble data assimilation for global oceanic climate studies. Mon Wea Rev 135:3541–3564